2PFC™ Image Sensors: Better Image Quality at Lower Cost

Douglas J. Tweet[a], Jong-Jan Lee[a], Jon M. Speigle[a], and Daniel Tamburrino[a,b]
[a]Sharp Laboratories of America, 5700 NW Pacific Rim Blvd, Camas, WA, USA 98607-9489;
[b]School of Computer and Communication Sciences, Ecole Polytechnique Fédérale de Lausanne (EPFL), CH-1015 Lausanne, Switzerland

ABSTRACT

A modification to the standard Bayer CFA and photodiode structure for CMOS image sensors is proposed, which we call 2PFC™, meaning "Two Pixel, Full Color". The blue and red filters of the Bayer pattern are replaced by magenta filters. Under each magenta filter are two stacked, pinned photodiodes; the diode nearest the surface absorbs mostly blue light and the deeper diode absorbs mostly red light. The magenta filter absorbs green light, improving color separation between the resulting blue and red diodes. The dopant implant defining the bottom of the red-absorbing region can be made the same as the green diodes, simplifying the fabrication. Since the spatial resolution for the red, green, and blue channels are identical, color aliasing is greatly reduced. Luminance resolution can also be improved, the thinner diodes lead to higher well capacity with resulting better dynamic range, and fabrication costs can be similar to or less than standard Bayer CMOS imagers. Also, the geometry of the layout lends itself naturally to frequency-based demosaicing.

Keywords: 2PFC™, stacked sensor, CMOS imager sensor, demosaicing, demosaicking, CFA, ISET

1. INTRODUCTION

To improve color accuracy, spatial resolution, reduce aliasing and demosaic artifacts, over the years a number of color filter array (CFA) patterns have been proposed as alternatives to the Bayer RGB pattern [1], a few of which [2-4] are illustrated in Fig. 1. Stacked pixel structures which make use of variation of the absorption depth with wavelength have also been proposed, both in Si [5-12] and a-Si alloy [13] systems. Most notable among these is the Foveon triple junction CMOS image sensors [8-10], in which R, G, and B information is collected at each pixel without the need for color filters, thus eliminating the demosaic algorithms and accompanying image artifacts. However, to achieve acceptable color separation the total Si absorbing region has to be quite deep, requiring expensive epitaxial Si processes.

A particularly interesting structure was investigated by Findlater, et al. [11]. They proposed a two-pixel stacked structure, using the Si depth to separate colors, but with the addition of color filters. Using a fairly complex 6T readout architecture they fabricated a prototype sensor with cyan and yellow filters. A system with magenta and green filters over alternate pixels was also briefly discussed, but they did not seem to develop it further. Another architecture with blue and red stacked sensors in one pixel and green in a separate pixel has also been proposed [12]. The device structure and depth of the blue and red diodes is similar to Foveon's; but the middle, green-absorbing region is pulled out and placed in an adjacent pixel. No color filters are employed, relying on the absorption depth to separate the colors. However, this design seems to have the same disadvantages of Foveon but with none of the advantages.

Here we propose a modification to the standard Bayer CFA and photodiode structure for CMOS image sensors which we call 2PFC™, meaning "Two Pixel, Full Color". It uses stacked blue and red sensors in one pixel with a single sensor in the adjacent green pixels. The difference from previous work [11,12], is that the device structure is completely compatible with standard CMOS processes, so fabrication costs, leakage, etc should be low.

In 2PFC™ the blue and red filters of the Bayer pattern are replaced by magenta filters, under which are two stacked, pinned photodiodes; the diode nearest the surface absorbs mostly blue light and the deeper diode absorbs mostly red light. The magenta filter absorbs green light, improving color separation between the stacked diodes. A number of benefits naturally occur from these modifications. Since the spatial resolution of green, red, and blue are identical color aliasing is greatly reduced and luminance resolution is improved, at least for simple demosaic schemes. Another advantage is higher well capacity, due to the thinner stacked diodes, leading to better dynamic range and signal-to-noise ratio. The reduction of color filters from three to two, while maintaining standard CMOS processing, keeps the overall cost similar or less than Bayer. The 2PFC™ design also lends itself naturally to frequency-based demosaic methods.

Here we present device structure, Nyquist limits, optical modeling of the color spectra, demosaicing, and system performance analysis.

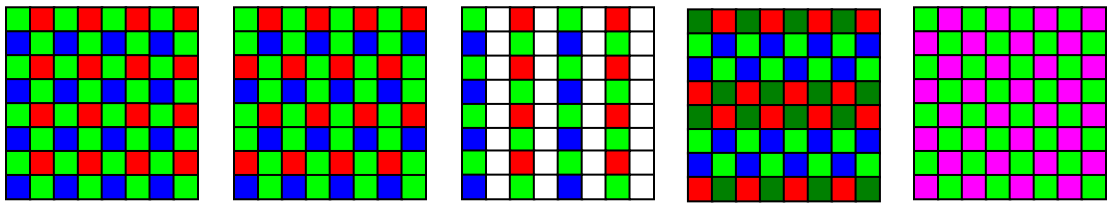

Fig. 1. Representative CFA patterns: (a) Bayer [1], (b) Lukac [2], (c) Kodak [3], (d) Hirakawa's 'Pattern A', [4] and (e) 2PFC™, the subject of this paper.

2. 2PFC™ DEVICE STRUCTURE

A conventional imager uses 3 pixels to detect 3 colors. 2PFC™ uses 2 pixels to detect 3 colors. Green is detected by the device under the green filter, blue and red are detected by the stacked devices under the magenta filter. Fig. 2 is a schematic of a cross-section of the device.

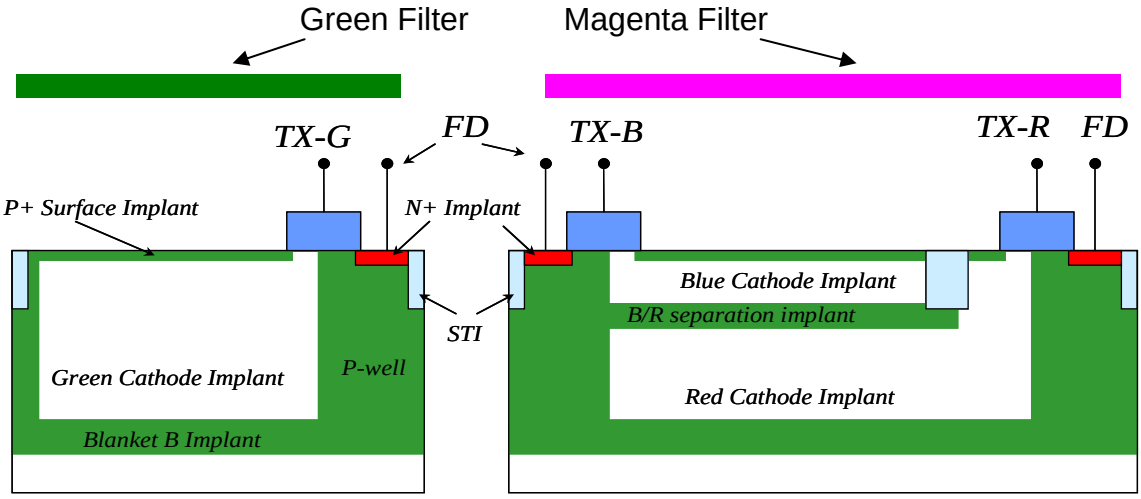

Fig. 2. Device structure of 2PFC™

On the left of Fig. 2 is shown the pixel for green light detection. The structure of this single junction pixel can be the same as that of current CMOS imagers, with a buried photodiode, transfer gate, and floating diffusion region. On the right side is shown the stacked junction pixel for blue and red detection. The blue and red absorbing regions are separated by a boron implant and by shallow trench isolation (STI). Complete charge transfer from the red diode to the floating diffusion can be realized through the careful design of the ion implant and the device layout. Since buried photodiode structures are used for all three detectors, dark current, reset noise and charge transfer are the same as standard CMOS sensors. Only 2-3 extra masks are needed for ion implantation, and one color filter is eliminated, so fabrication costs should be the same or less than standard CMOS image sensors. Due to the thinner red and blue diodes, the full well capacity will be higher than the usual single diode. Simulations indicate that 2-3 times higher capacities can be obtained. Combined with the expectation that the noise should be similar to the standard structure, both dynamic range and signal-to-noise ratio should have a corresponding 2-3x improvement.

In order to increase the green diode capacitance, an anode (p-doped region) can be inserted in the middle of the green cathode, creating a split structure. This has already been shown to be feasible in a standard CMOS structure [14] and gives a ~1.5x improvement in full well capacity, improved signal-to-noise ratio, very low V_{pin}, and low crosstalk without any degradation of dark current and image lag performance. In order to fabricate a device with this structure in standard CMOS, a minimum of one more mask step is needed. In the case of 2PFC™, this step is the same as the R/B separation implant, so no extra process steps are needed to fabricate a green photodiode with high full well capacity. The modified green pixel has 2-3 times higher capacitance. Readout architecture for 2PFC™ is similar to the standard shared pixel APS circuit. In conventional CMOS imager, the APS circuit is shared between either 2 pixels or 4 pixels. For 2PFC™, the APS circuit is shared between 3 pixels, namely, the red, green, and blue pixels.

3. COMPARISON OF BAYER AND 2PFC™ CFA NYQUIST LIMITS

In the standard Bayer CFA (Fig 1(a)), half of the pixels detect green light, giving a green sampling rate of 50%, while the red and blue sampling rates are each only 25%. However, for the 2PFC™ CFA (Fig 1(e)) the sampling rates for all three color channels are 50%. This allows 2PFC™ to have higher luminance resolution than Bayer for the same pixel pitch, at least with simple demosaic algorithms, such as bilinear, but it also greatly reduces color aliasing.

Nyquist maps for Bayer and 2PFC™ are compared in Fig. 3. Bayer has higher Nyquist frequency in the horizontal and vertical directions than along the diagonal, while red and blue are the converse. In comparison, for 2PFC™ the green, red, and blue Nyquist frequencies are all identical, and are highest along the horizontal and vertical directions. This is highly desirable, since the resolution differences for Bayer increase color aliasing. Also, the human visual system has higher spatial resolution in the horizontal and vertical directions than along the diagonal direction (Fig. 4). The Bayer CFA green matches the human eye 2D contrast sensitivity function (CSF), but red and blue do not. For the 2PFC™ pattern, all three colors match the eye's CSF.

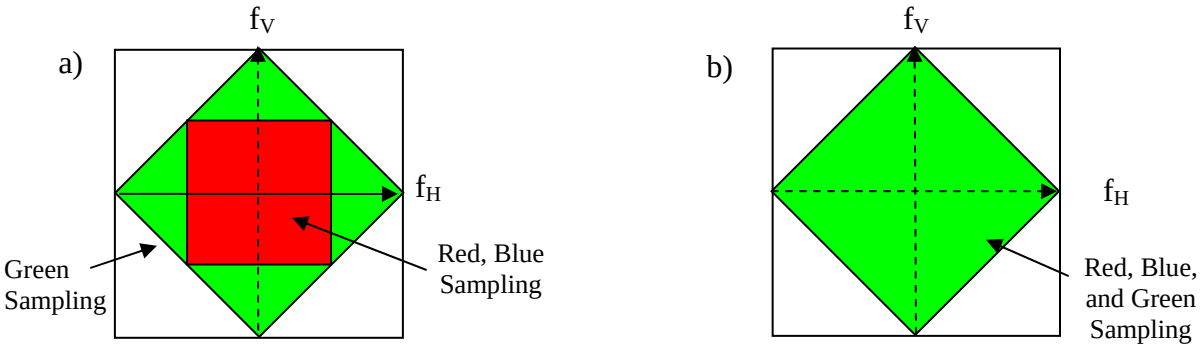

Fig. 3. Nyquist spatial frequency limits for (a) Bayer and (b) 2PFC™ in the horizontal and vertical directions. f_H and f_V are the spatial frquencies in the horizontal and vertical direction, respectively.

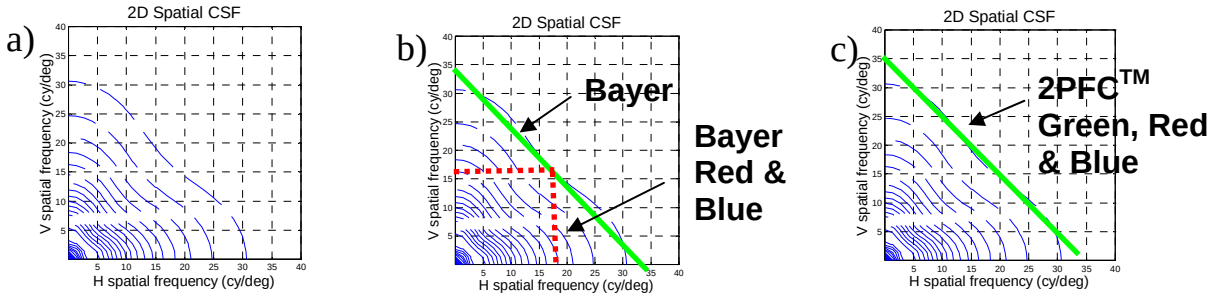

Fig. 4.(a) Human eye 2D spatial contrast sensitivity function (CSF). Comparison of CSV with Nyquist limits for (b) Bayer and (c) 2PFC™, corresponding to 1st quadrant of plots in Fig 3.

4. OPTICAL MODELING OF COLOR SPECTRA

Estimates of the color spectra for the stacked blue and red diodes were calculated using commercial optical thin film software [15]. In the example shown in Fig. 5(a), a simplified dielectric stack was used, consisting of just a silicon nitride layer. The silicon beneath the dielectric was divided into four layers, corresponding to Fig 2: a thin heavily p+ doped Si film on top, a mostly blue-absorbing region, a mostly red-absorbing region, and the Si substrate. Referring to Fig. 2, the boundary between the blue- and red-absorbing regions is roughly in the middle of the B/R separation implant. The software can calculate the absorptance of a given Si layer, which is the fraction of incident photons absorbed in that layer at a given wavelength. Each absorbed photon produces an electron/hole pair, and if each of these is collected by the circuitry (and not lost to recombination, defect traps, etc), then the calculated optical absorptance will correspond to external electronic quantum efficiency. In the model shown in the inset to Fig. 5(a), specific thicknesses of the various Si layers were assumed and the absorptances of the layers calculated, which were then multiplied by the transmittances of a magenta color filter and an IR-cut filter (removing incident light beyond 700nm). The quantum efficiencies of the "Blue Si" and "Red Si" layers are shown. As expected, there is some color mixing between the blue and red channels which will require correction in the image processing software. The extent of this color mixing and methods to reduce it will depend on details of the structure of the different Si layers as well as on the actual dielectric stack used. Two sets of RGB spectra were used in image simulations to test the effect of variation in spectra. Fig. 5(b) and 5(c) show cases in which the maxima of the red and blue peaks are the same as or 1/3 lower than the green maximum, respectively.

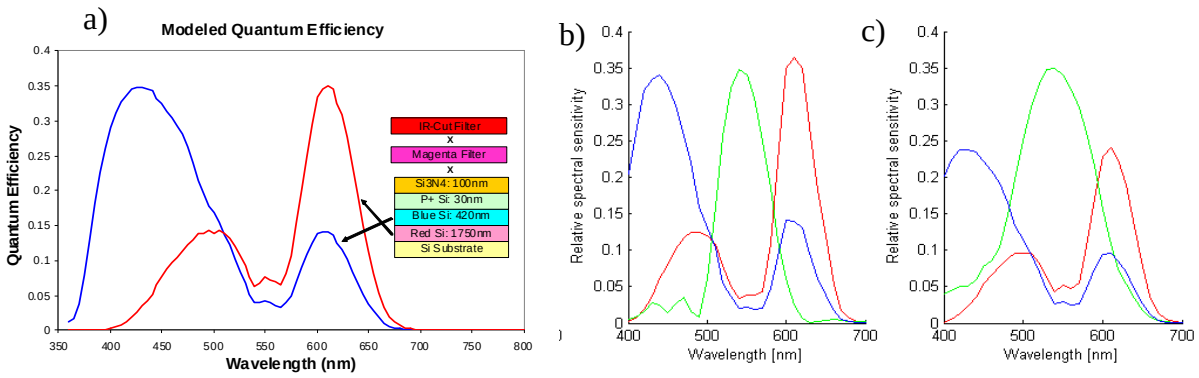

Fig. 5 (a) Modeled quantum efficiency of the stacked "blue" and "red" photodiodes calculated using optical methods [15]. Sensor spectral sensitivity responses used in image simulations to represent (b) equivalent RGB strengths (referred to as 'FiltG' in later sections and figures) and (c) weaker RB responses (referred to as 'RGB3').

Large individual and stacked photodiodes (PDs) were fabricated and the quantum efficiency measured as a function of wavelength. QE was determined by measuring the current from PDs illuminated by light from 350nm to 1000nm, and comparing the result with current from a reference PD with known QE, correcting for diode area. The QE measured in this fashion for an individual PD is shown in Fig. 6(a), along with the modeled QE using the optical method described above and the structure given in the inset. From ~400nm to 1000nm the model matches the data very well. Below 400nm the incident light is very weak and the data less reliable. Fig. 6(b) compares the electrically determined QE and optically modeled QE for stacked "blue" and "red" PDs on the same wafer. The model structure is the same as for Fig. 6(a), except that the 1450nm thick "green" region in Fig 6(a) is split into 350nm for "blue" and 1100nm for "red". The models agree with the data quite well, indicating there is no "dead" region between the blue and red cathodes. Photons absorbed in the B/R separation implant layer (see Fig. 2) will go to one or the other cathode and be collected.

QE measurements on devices with green and magenta color filters are shown in Fig. 6(c) and 6(d), respectively. Fig. 6(c) shows the same device as in Fig 6(a) before and after addition of a green filter. Reduction in the peak intensity is a little more than would be expected by the transmittance curve provided by the filter vendor, suggesting some destructive interference. Fig. 6(d) plots the effect of a magenta filter on stacked diodes (not the same wafer as Fig. 6(b). Observe that both the blue and red PDs covered by the filter have QE higher than the unfiltered curves at some wavelengths, suggesting an interference effect. The aforementioned color mixing is evident in the filtered curves. The amount of red light absorbed by the "blue" PD is fairly small, but the "red" PD has more of a problem. Clearly, the main "red" peak is too weak, indicating the red cathode is too thin. A deeper blanket boron implant (see Fig. 2) will improve this.

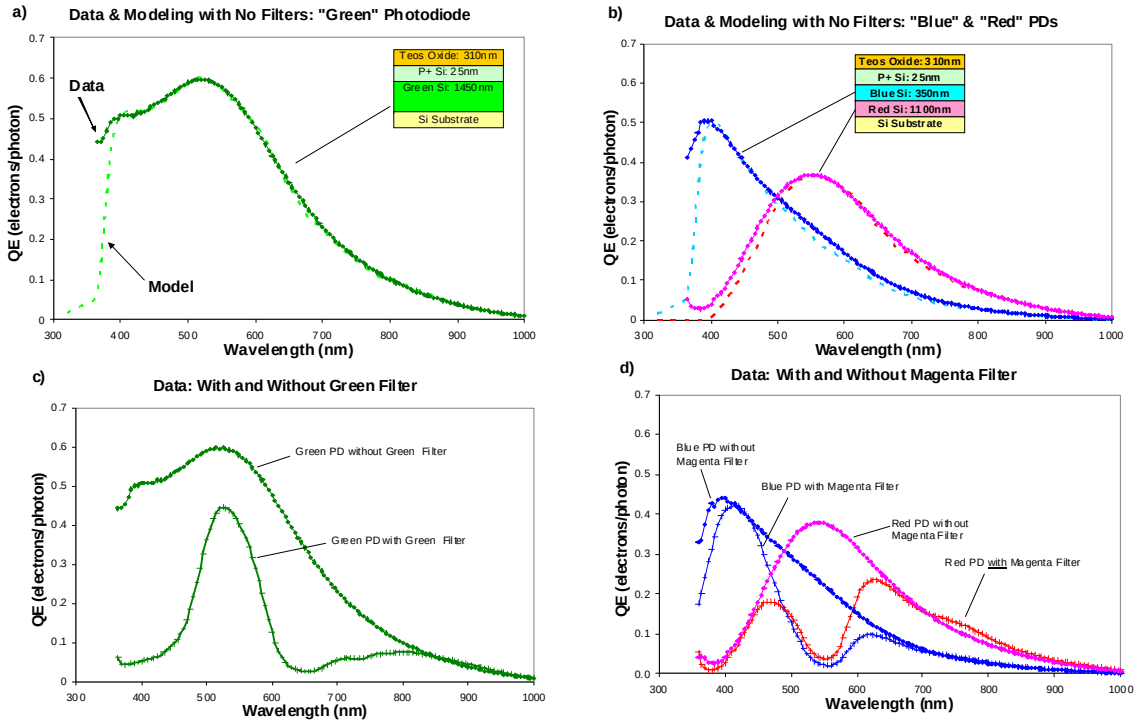

Fig. 6 QE measured from photocurrent (solid symbols) and modeled optically (dashed lines) for (a) an individual green diode and (b) stacked blue and red diodes, without color filters. Measured QE with and without color filters for the (c) green diode and (d) stacked blue and red diodes.

5. DEMOSAICING FOR 2PFC™

In 2005, Alleysson et al.[16] proposed a demosaicing method based on a frequency domain approach. They showed that for a Bayer CFA pattern, the CFA signal can be decomposed into luminance and modulated chrominance components. Fig. 7(a) shows for a Bayer CFA how the luminance and chrominance information in the CFA image are separated in a frequency-domain representation. The luminance information is located at lower frequencies (center) while the chrominance information is located at higher frequencies (borders and corners). This separation suggested demosaicing by first separating luminance from chrominance using linear filtering followed by reconstructing chrominance information via interpolation. The results of this method depend strongly on the filter used to extract the luminance and chrominance information from the CFA. As there usually is non-negligible cross-talk between luminance and chrominance information, this method can result in reconstructed images exhibiting color aliasing and other artifacts. Alleysson et al.[16] described the four main types of artifacts as blurring, color aliasing, grid effect, and watercolor effect. Subsequently, Dubois [17] and Lian et al. [18] proposed enhancements that improved the results by adaptively filtering the luminance component. Recent research to improve these frequency-based methods has explored designing non-Bayer CFA patterns in order to maximize the separation between luminance and chrominance information in the frequency domain, thus reducing cross-talk [4, 19].

5.1 Frequency Analysis of 2PFC™ [G R/B] Pattern

The location of the chrominance information was first derived for a Bayer pattern by Alleysson [16] and then by Dubois [17] using different notations. Using Dubois' notation, we derive the frequency representation of the 2PFC™ pattern. Since red and blue pixels are co-sited with 2PFC™, we consider two mosaiced patterns, [G R] and [G B]. Due to these sub-arrays having the same pattern, the derivation will be done only for [G R] as it is similar for [G B].

Let $f_G[i,j]$ and $f_R[i,j]$ be the green and red channels of the original image and $f_{CFA}[i,j]$ the output of our 2PFC™ sensor at pixel location [i,j]. $f_{CFA}[i,j]$ is obtained by sub-sampling the $f_G[i,j]$ and $f_R[i,j]$ functions to match the CFA pattern. The sub-sampling can be represented by a multiplication by the functions $m_k[i,j]$, $k \in \{G,R\}$ that take a value 1 or zero (eqn 1) (see Table 1).

Table 1. Equations (1) – (5) for the frequency analysis of the 2PFC™ [G R/B] pattern.

$m_G[i,j]=\frac{1}{2}(1+(-1)^{i+j})$ $m_R[i,j]=\frac{1}{2}(1+(-1)^{i+j+1})$ (1)	$f_{CFA}[i,j]=\frac{1}{2}f_G[i,j](1+(-1)^{i+j})+\frac{1}{2}f_R[i,j](1+(-1)^{i+j+1})$ (2)
$f_{CFA}[i,j]=\frac{1}{2}[f_G[i,j]+f_R[i,j]]+\frac{1}{2}(-1)^{i+j}[f_G[i,j]-f_R[i,j]] \coloneqq f_L[i,j]+f_C[i,j](-1)^{i+j}$ (3)	
$f_{CFA}(i,j)=f_L[i,j]+f_C[i,j]\exp(2\pi\sqrt{-1}(i+j)/2)$ (4)	$F_{CFA}(u,v)=F_L(u,v)+F_C(u-0.5,v-0.5)$ (5)

With these modulation functions, the CFA signal $f_{CFA}[n,m]$ can be written as in eqn. (2) and rearranged as eqn. (3), where f_L is a fully sampled signal associated with luminance and f_C is a modulated signal defined as chrominance. Noting that $-1=\exp(j\pi)$, the decomposition is given in eqn. (4) and its Fourier transform in eqn. (5).

Comparing this result with that of the Bayer pattern (Fig. 7(a) and (b)), we note that 2PFC™ has only one kind of modulated chrominance information. It is located at the corners of the Fourier spectrum, i.e. at high frequencies, thus maximizing the separation between luminance and chrominance. The location of the chrominance and the little amount of cross-talk permit the usage of a simpler separation filter than those used for a Bayer CFA. An example of a filter and its frequency response is given in Fig. 7(c) and 7(d).

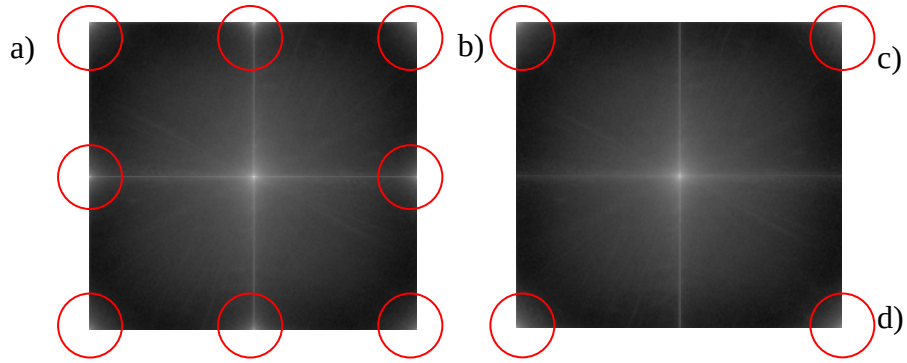

$$\frac{1}{64}\begin{bmatrix} 0 & 1 & -2 & 1 & 0 \\ 1 & -4 & 6 & -4 & 1 \\ -2 & 6 & 56 & 6 & -2 \\ 1 & -4 & 6 & -4 & 1 \\ 0 & 1 & -2 & 1 & 0 \end{bmatrix}$$

Fig. 7. Mean representation of the log magnitude of the Fourier transform for the 24 Kodak images with (a) Bayer CFA: chrominance is located at borders and corners. (b) 2PFC™ CFA: chrominance is located at corners only. (c) 5x5 luminance extraction filter, and (d) corresponding filter frequency response.

5.2 Proposed Demosaicing Algorithm

With the 2PFC™ CFA, the red and blue color information have the same spatial location. We take the approach of separating the CFA information into two channels [G R] and [G B] and processing them similarly.

Table 2. Equations (6) – (9) for the frequency-based demosaicing method of the 2PFC™ [G R/B] pattern.

$f_L^{GR} = h_L * f_{CFA}^{GR}$ $f_L^{GB} = h_L * f_{CFA}^{GB}$ (6)	$f_C^{GR} = f_{CFA}^{GR} - f_L^{GR}$ $f_C^{GB} = f_{CFA}^{GB} - f_L^{GB}$ (7)	$f_L^G = \left(f_{CFA}^{GR} + f_L^{GR}\right)/2$ $f_C^G = \left(f_C^{GR} + f_C^{GB}\right)/2$ (8)	$\hat{f} = L + \hat{C}$ (9)

Let f_{CFA}^{GR} and f_{CFA}^{GB} be the two above-mentioned mosaiced channels and h_L the luminance extraction filter. In a first step h_L is applied to f_{CFA}^{GR} and f_{CFA}^{GB} respectively as shown in eqn. (6) (see Table 2). The multiplexed chrominance component is estimated by subtracting the above luminance from the CFA signal as shown in eqn. (7).

The green channel is handled differently as it is present in both f_{CFA}^{GR} and f_{CFA}^{GB}. The luminance and multiplexed chrominance are defined as the average of the values extracted from the two mosaics (eqn. 8). Letting $L = \left(f_L^{GR}, f_L^G, f_L^{GB}\right)$ be the 3-channel extracted luminance and $C = \left(f_C^{GR}, f_C^G, f_C^{GB}\right)$ be the 3-channel multiplexed chrominances, the chrominance channels in C are de-multiplexed according to the CFA pattern and the missing values are reconstructed using bilinear interpolation to form $\hat{C}$. Finally, the full color image $\hat{f}$ is reconstructed by adding the chrominance channels to their respective luminance channels, eqn. (9).

5.3 Filter Design

In our proposed demosaicing algorithm, we use the filter h_L to extract luminance from the CFA image (Eqn. 6). The filter was computed by defining a standard least-squares problem [20], $h_L = \arg\min_h E\left[\left(f_L - h * f_{CFA}\right)^2\right]$, where f_{CFA} is the CFA image and f_L the luminance image. In practice, the error is minimized over a training set of full color images and f_L is thus known. The luminance extraction filter h_L was estimated using the Kodak RGB image set. When implemented in a full digital camera workflow, the filter will need to be re-computed based on sensor data to account for the effect of the color filters' spectral sensitivities.

5.4 Results

In this section, we present experimental results from several demosaicing algorithms applied on Bayer CFA and 2PFC™ [G~R/B] CFA. The Bayer algorithms were chosen based on performance and on availability of a reference implementation, and include: bilinear interpolation, Lian et al's adaptive filtering (AF) [18], Zhang and Wu's DLMMSE (DL) [21], Gunturk et al's alternating projections (POCS) [22], Menon and Calvagno's wavelet based method (DBW) [23], and Menon et al's directional filtering (DFPD) [24]. The 2PFC™ algorithms are: bilinear interpolation, frequency-based method with 5x5 (F5) or 21x21 (F21) filters, and a directional spatial-domain method. In Table 3, some algorithms' names are followed by a + sign, indicating that a 3x3 median filter was applied as a post-processing step.

The algorithms were applied to the commonly-used 24 Kodak PhotoCD images after sub-sampling according to the CFAs. Sample results can be seen in Fig. 8. Values of several image quality metrics are reported in Table 3, and include PSNR ($PSNR = 10 \log_{10}\left(255^2/MSE\right)$), S-CIELAB ΔE [25], and Lu & Tan's zipper metric [26]. Zhang & Wandell's S-CIELAB color difference metric is an extension of standard CIELAB ΔE that takes into account the spatial frequency sensitivities of the human visual system. Lu and Tan's zipper metric is aimed at quantifying alternating patterns in smooth regions near edges. The metric values are computed after removing a 5-pixel border from each image in order to discount errors due to unhandled edge effects. As suggested by Lu & Tan [26], the metrics are also computed separately for the smooth and edge regions of the reconstructed image. This separation yields a sense of relative performance in these two types of region.

Metrics for 2PFC™ demosaiced images outperform the Bayer-based methods. PSNR is more than 4dB higher, color difference is almost half, and zipper effect is up to three times less for 2PFC™ than Bayer. These results are observed for both edge and smooth regions.

Among other things that can be seen from the results, median filtering greatly reduce zipper artifacts and use of a 5x5 filter in the frequency domain method doesn't penalize the results relative to a larger 21x21 filter.

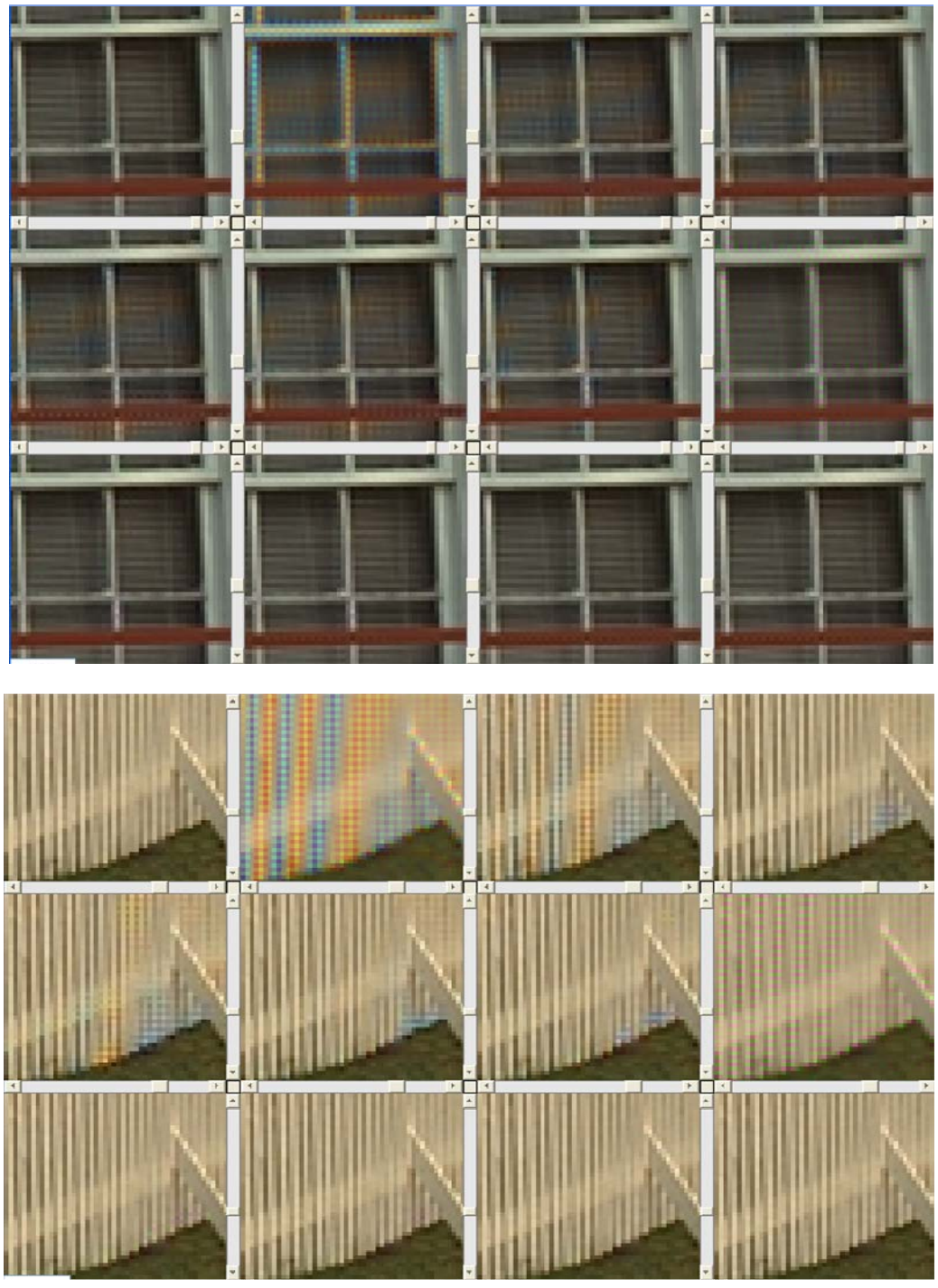

Fig. 8. Cropped regions from two Kodak images. Within each set, left-to-right and top-to-bottom: (1) original, (2) [Bayer] bilinear, (3) [Bayer] adaptive filtering (AF), (4) [Bayer] DLMMSE (DL), (5) [Bayer] POCS, (6) [Bayer] DBW, (7) [Bayer] DFPD, (8) [2PFC] bilinear, (9) [2PFC] spatial method, (10) [2PFC] spatial method + median, (11) [2PFC] frequency method 5x5, (12) [2PFC] frequency method 5x5 + median

Table 3. PSNR(dB), S-CIELab ΔE, and zipper effect metrics of different demosaicing algorithms for Bayer [B] and 2PFC [2] on Kodak PhotoCD image set. Each metric is computed for the full image, smooth regions, and edge regions.

	Full Image			**Smooth Region**			**Edge Region**		
	PSNR	**ΔE**	**Zip**	**PSNR**	**ΔE**	**Zip**	**PSNR**	**ΔE**	**Zip**
[B] Bilinear	30.2	1.70	35.4	34.5	1.38	29.0	22.9	8.58	77.6
[B] AF	39.6	0.82	3.43	41.5	0.80	2.14	34.3	3.15	9.99
[B] DL	40.0	0.79	2.96	42.0	0.76	1.86	34.7	3.09	8.99
[B] POCS	39.3	0.90	2.76	41.1	0.87	1.73	34.0	3.44	8.60
[B] DBW	39.7	0.84	3.33	41.7	0.82	1.95	34.3	3.22	10.9
[B] DFPD	39.3	0.88	5.01	41.3	0.84	3.42	33.9	3.34	13.5
[B] DFPD+	39.6	0.86	2.85	41.6	0.82	1.77	34.3	3.36	8.79
[2] Bilinear	33.2	1.08	35.4	37.3	0.93	30.0	26.0	4.90	73.1
[2] Directional	43.3	0.57	3.98	45.1	0.56	2.57	38.1	2.17	11.9
[2] Directional+	44.1	0.55	1.20	45.8	0.53	0.62	39.1	2.15	4.67
[2] F5	43.9	0.51	2.07	45.8	0.50	1.14	38.6	2.04	7.31
[2] F21	44.3	0.49	1.34	46.1	0.47	0.70	39.1	1.96	5.10
[2] F5+	44.3	0.52	1.10	46.1	0.50	0.56	39.2	2.09	4.31
[2] F21+	44.5	0.50	1.01	46.2	0.48	0.52	39.4	2.04	3.98

6. SYSTEM PERFORMANCE ANALYSIS

Overall system performance of a 2PFC^{TM} sensor was evaluated using a simulated imager and image processing pipeline, utilizing Farrell et al.'s ISET Matlab environment [27]. ISET allows specifying scene spectral, camera optical, and sensor parameters including spectral sensitivity and noise behavior. Our simulations used sensor geometries and noise parameters typical of cell phone cameras but with diffraction-limited optics. Common noise parameters were used for the Bayer and 2PFC^{TM} CFAs, as an accurate 2PFC^{TM} noise model is not available at this time. The image processing components of the pipeline included demosaicing, white-balancing, and color correction to the sRGB colorspace.

6.1 Resolution

In terms of spatial resolution, a 2PFC^{TM} stacked sensor can be expected to have slightly better performance than a Bayer array at the same pixel pitch. But the expected difference may not be large, as 1) the R and B contribution to luminance is lower than G and 2) the [G RB; RB G] 2PFC^{TM} geometry has the same green sampling rate as a Bayer CFA. Additionally, spatial resolution also depends strongly on the demosaicing method.

To evaluate the Bayer and 2PFC^{TM} resolution performance, we analyzed simulated images of the ISO12233 slanted bar target and report MTF50 values. Fig. 9 presents the derived MTF curves for the R, G, and B channels. The black curve represents the luminance MTF response. For bilinear demosaicing (Fig 2(a) and (b)), 2PFC^{TM} performs better than Bayer in terms of MTF50 values and the R, G, and B MTF curves are coincident. However, when using state-of-the-art demosaicing algorithms, the resolution difference as measured by the MTF becomes much smaller. Fig. 9(c) compares Menon et al.'s method [24] with our frequency-based 2PFC^{TM} method in Fig. 9(d). Both give similar, much higher MTF50 values than the bilinear cases. Also, the Menon et al. method does quite well for this black-and-white edge at equating the MTF responses of the R, G, and B channels (mainly due to how it equates the high frequency content between R, G, and B channels), while 2PFC^{TM} exhibits some spread. Thus, using a more-sophisticated demosaicing method for Bayer leads to a much sharper resulting image and with resolution comparable to that of a 2PFC^{TM}-based method. 2PFC^{TM} can, therefore, be considered to have higher resolution only when using low-complexity demosaicing.. This slanted-bar resolution measure, however, does not necessarily indicate which demosaicing method is of better quality as Bayer tends to have more color artifacts than 2PFC^{TM} (e.g. see Fig. 8).

We also evaluated resolution using a method stipulated by the Camera & Imaging Products Association (CIPA) [28]. With ISET we simulated images of the J1 region of the ISO12233 test chart as if the chart were ~100cm from the camera, Fig. 10. These images were then input into the "HYRes" software downloaded from the CIPA website. This software analyzes the images and determines the point at which the 5 lines in the J1 test pattern become unresolved, indicated by the red line in each image. Fig. 10 shows Bayer images for bilinear, and Menon demosaicing, and 2PFC^{TM} with bilinear, spatial, and frequency-based demosaicing. The calculated resolution is 135 lines/picture-height (l/ph) for

Bayer with bilinear demosaicing, but improves dramatically to ~175 l/ph for all the rest, including 2PFC^{TM} with bilinear demosaic. Visually, the improvement is also impressive.

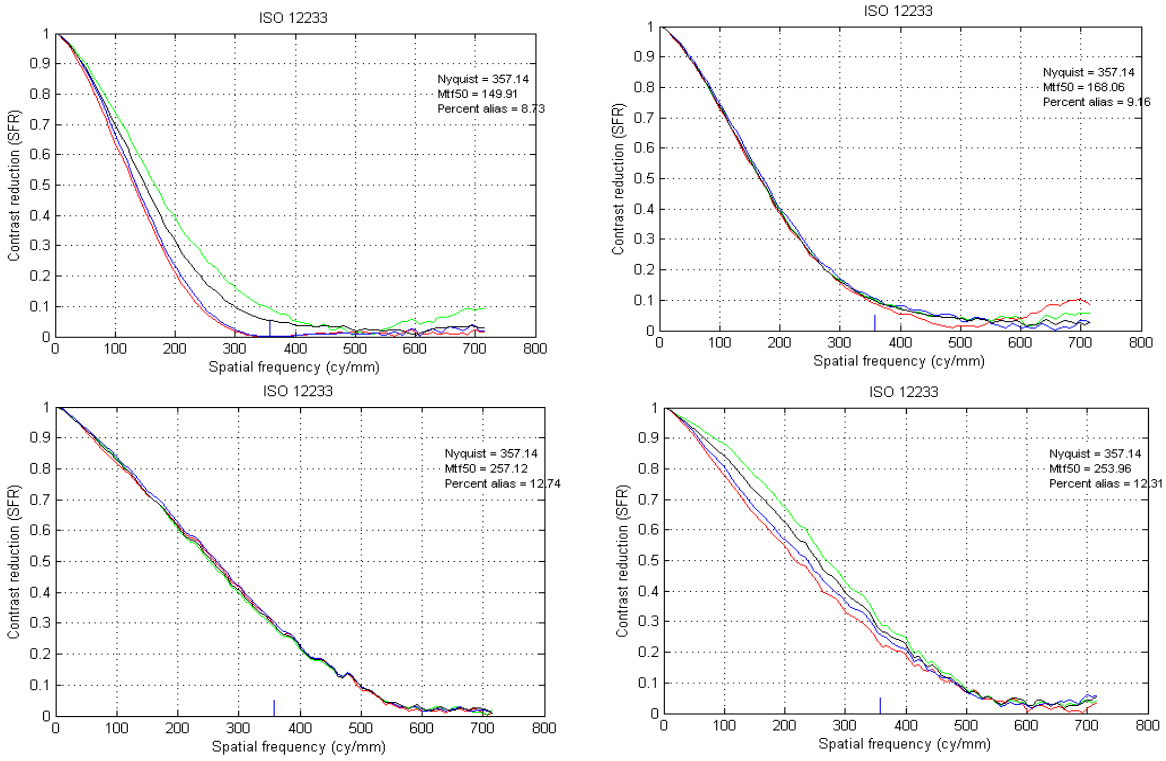

Fig. 9. R,G,B, and luminance MTF curves of simulated system after demosaicing for (a) Bayer with bilinear demosaicing, MTF50 ~150, (b) 2PFC^{TM} with bilinear demosaicing, MTF50~168, (c) Bayer with state-of-the-art demosaicing, MTF50~257, and (d) 2PFC^{TM} with our frequency-based demosaicing, MTF50~254. All used 1.40µm pixel pitch. The 'FiltG' spectra was used for 2PFC^{TM}, shown in Fig. 5(b).

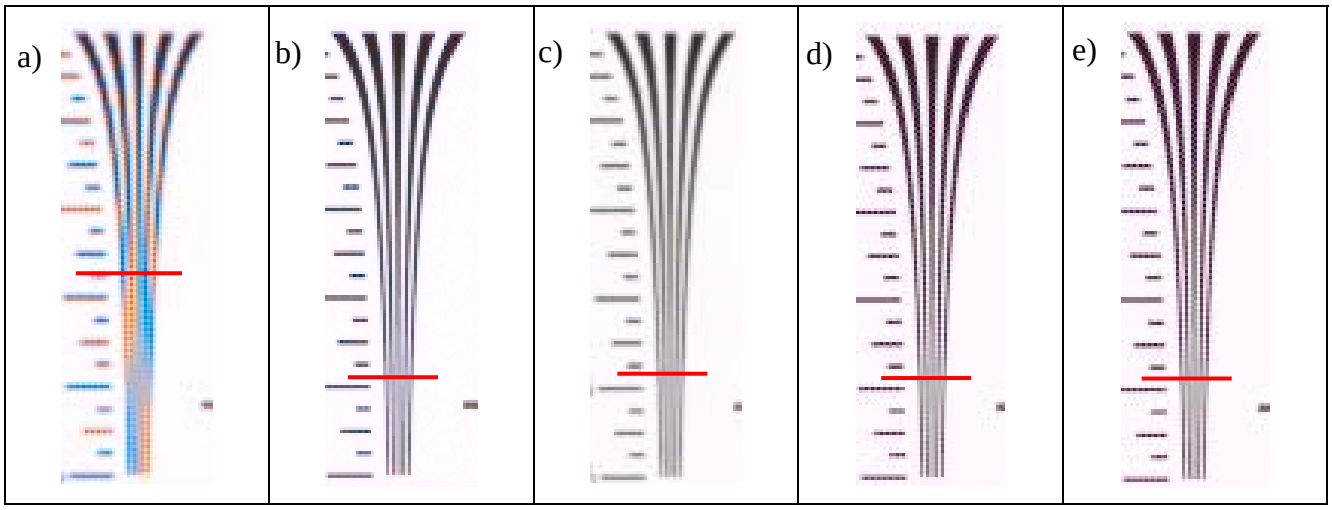

Fig. 10. ISET simulations of the J1 region of the ISO12233 chart, with resolution analyzed by "HYRes" according to the CIPA standard and indicated by the red lines . (a) Bayer, Bilinear, 135 l/ph, (b) Bayer, Menon, 176 l/ph, (c) 2PFC^{TM}, Bilinear, 174 l/ph, (d) 2PFC^{TM}, spatial demosaic, 177 l/ph, (e) 2PFC^{TM}, Frequency-based demosaic, 177 l/ph. All simulations used 1.55µm pixel pitch. The 'FiltG' spectra was used for 2PFC^{TM}, shown in Fig. 5(b).

6.2 Noise

ISET simulates several noise sources, including dark current, read noise, dark signal non-uniformity (DSNU), and photo response non-uniformity (PRNU). Noise parameters are kept the same for Bayer and 2PFC™ as we don't have yet an accurate noise model of 2PFC™, nor a prototype to measure it. The main source of noise level difference in the simulated results comes from the different color filters' spectral sensitivity response and from the color matrixing to convert from camera RGB values to a standard RGB color space. The spectral sensitivity curves of 2PFC™ filters (Fig. 5) are more correlated as the wavelength separation for the stacked pixel is not perfect and some reddish (bluish) light is captured in the blue (red) sensitive area of the pixel.

Noise was measured on the 18% gray level patch from a simulated Macbeth color checker under D65 rendered to sRGB. The noise is computed as the standard deviation divided by the mean value for both luma Y and chroma CbCr of the YCbCr color space. Fig. 11 shows the variation of noise with exposure time. At low exposures, luma noise is lower for 2PFC™ than for Bayer. A justification can be found in the higher quantum efficiency of the 2PFC™ color filters' spectral sensitivities response. Chroma noise is higher for 2PFC™ as the three color channels are more correlated, which leads to larger terms in the color-matrixing, thus amplifying noise.

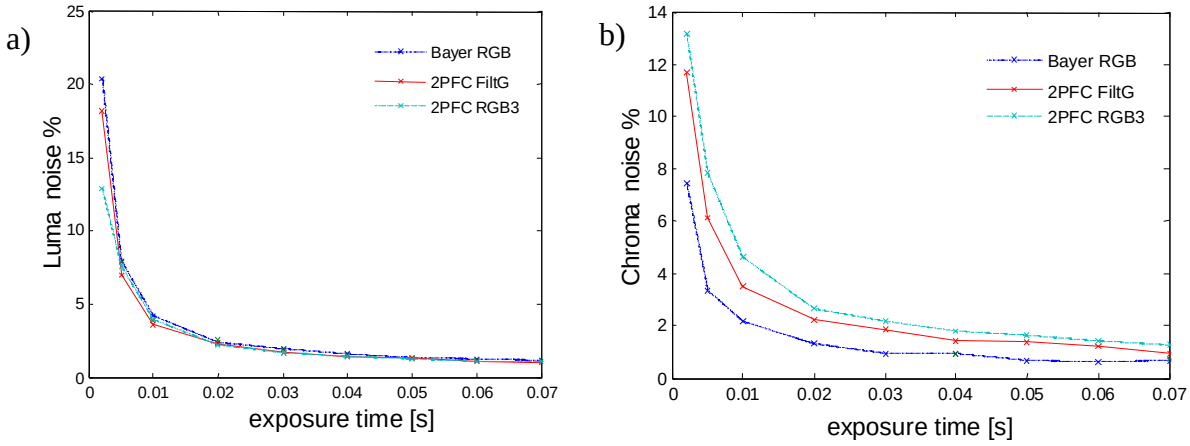

Fig. 11. (a) Luma and (b) chroma noise of a simulated 1.4µm pixel sensor at varying exposure time for Bayer-based and 2PFC™-based sensors with different color filters' spectral sensitivity response.

7. CONCLUSIONS

We have presented a modification to the standard Bayer CFA and photodiode structure for CMOS image sensors which we call 2PFC™, meaning "Two Pixel, Full Color". It uses stacked blue and red sensors in one pixel covered with a magenta filter, and a single sensor in the adjacent pixel covered by green filters. We have presented device structure, Nyquist limits, optical modeling of the color spectra, demosaicing, and system performance analysis. A number of benefits naturally occur from this design. Since the spatial resolution of green, red, and blue are identical color aliasing is greatly reduced and luminance resolution is improved, at least for simple demosaic schemes. Another advantage is higher well capacity, due to the thinner stacked diodes, leading to better dynamic range and signal-to-noise ratio. The reduction of color filters from three to two, while maintaining standard CMOS processing, keeps the overall cost similar or less than Bayer. The 2PFC™ design also lends itself naturally to frequency-based demosaic methods.

REFERENCES

[1] Bayer, B.E., "Color imaging array." US Patent 3 971 065, July 20, 1976.

[2] Lukac, R. and Plataniotis, K.N. "Color filter arrays: Design and performance analysis", IEEE Trans. Consumer Electron. 51, 1260-1267 (2005).

[3] Kijima, T., Nakamura, H., Compton, J.T. and Hamilton, J.F. Jr, “Image sensor with improved light sensitivity”, US Patent Application 20 070 177 236 (2007).
[4] Hirakawa, K. and Wolfe, P.J. “Second-generation color filter array and demosaicking designs”, Proc. SPIE 6822, 68221P, (2008).
[5] Carr, W.N. “Multi-spectrum photodiode devices”, US Patent 4 238 760, (1980).
[6] Harada, N. and Yoshida, O., “Visible/infrared imaging device with stacked cell structure”, US Patent 4 651 001, (1987).
[7] Seitz, P., Leipold, D., Kramer, J. and Raynor, J.M., “Smart optical and image sensors fabricated with industrial CMOS/CCD semiconductor processes”, Proc. SPIE 1900, 21-30 (1993).
[8] Merrill, R.B., “Color separation in an active pixel cell imaging array using a triple-well-structure,” US Patent 5 965 875, (1999).
[9] Gilblom, D.L., Yoo, S.K., Ventura, P. “Operation and performance of a color image sensor with layered photodiodes”, Proc. SPIE 5074, 318-331 (2003).
[10] Hubel, P.M., Liu, J. and Guttosch, R.J., “Spatial frequency response of color image sensors: Bayer color filters and Foveon X3”, Proc. SPIE 5301, 402-407 (2004).
[11] Findlater, K.M., Renshaw, D., Hurwitz, J.E.D., Henderson, R.K., Purcell, M.D., Smith, S.G. and Bailey, T.E.R., “A CMOS image sensor with a double-junction active pixel”, IEEE Trans. on Electron Devices, 50(1), 32-42 (2003).
[12] Hong, S., “CMOS image sensor and method of fabrication”, US Patent 6 946 715, (2005).
[13] Steibig, H., Street, R.A., Knipp, D., Krause, M. and Ho, J., “Vertically integrated thin-film color sensor arrays for advanced sensing applications” Appl. Phys. Lett. 88, 013509 (2006).
[14] Lim, Y., Lee, K., Hong, H., Kim. J., Sa., S., Lee, J., Kim. D. and Hynecek, J. “Stratified photodiode: a new concept for small size-high performance CMOS image sensor pixels”, 2007 Image Sensor Workshop, 311-314 (2007).
[15] *The Essential Macleod*, Thin Film Center, Inc., Tucson, Arizona.
[16] Alleysson, D., Süsstrunk, S., and Hérault, J., "Linear demosaicing inspired by the human visual system," IEEE Transactions on Image Processing 14(4), 439-449 (2005).
[17] Dubois, E., "Frequency-domain methods for demosaicking of bayer-sampled color images," IEEE Signal Processing Letters 12, 847-850 (December 2005).
[18] Lian, N., Chang, L., and Tan, Y.-P., "Improved color filter array demosaicking by accurate luminance estimation.," IEEE Intl. Conf. Im. Proc. (vol 1), 41-44 (2005).
[19] Alleysson, D. and Chaix de Lavarène,, B., "Frequency selection demosaicking: A review and a look ahead," Proc. SPIE 6822, 68221M (2008).
[20] Dubois, E., "Filter design for adaptive frequency-domain bayer demosaicking," IEEE Intl. Conf. Im. Proc., 2705-2708 (2006).
[21] Zhang, L. and Wu, X., "Color demosaicking via directional linear minimum mean square-error estimation," IEEE Trans. Image Processing 14, 2167-2178 (December 2005).
[22] Gunturk, B. K., Altunbasak, Y., and Mersereau, R. M., "Color plane interpolation using alternating projections.," IEEE Transactions on Image Processing 11, 997-1013 (September 2002).
[23] Menon, D. and Calvagno, G., "Demosaicing based on wavelet analysis of the luminance component," IEEE Intl. Conf. Im. Proc. (vol. 2), 181-184 (2007).
[24] Menon, D., Andriani, S., and Calvagno, G., "Demosaicing with directional filtering and a posteriori decision.," IEEE Transactions on Image Processing 16(1), 132-141 (2007).
[25] Zhang, X. and Wandell, B. A., "A spatial extension of cielab for digital color image reproduction," in Proc. of the SID Symposiums, 731-734 (1996).
[26] Lu, W. and Tan, Y.-P., "Color filter array demosaicking: new method and performance measures.," IEEE Transactions on Image Processing 12(10), 1194-1210 (2003).
[27] Farrell, J. E., Xiao, F., Catrysse, P. B., and Wandell, B. A., "A simulation tool for evaluating digital camera image quality," Proc. SPIE 5294, 124-131 (2004).
[28] “CIPA DC-003-Translation -2003, Resolution Measurement Methods for Digital Cameras”, Camera and Imaging Products Association (CIPA), Dec. 17, 2003.